

# Chemical Science

Accepted Manuscript



This is an *Accepted Manuscript*, which has been through the Royal Society of Chemistry peer review process and has been accepted for publication.

*Accepted Manuscripts* are published online shortly after acceptance, before technical editing, formatting and proof reading. Using this free service, authors can make their results available to the community, in citable form, before we publish the edited article. We will replace this *Accepted Manuscript* with the edited and formatted *Advance Article* as soon as it is available.

You can find more information about *Accepted Manuscripts* in the [Information for Authors](#).

Please note that technical editing may introduce minor changes to the text and/or graphics, which may alter content. The journal's standard [Terms & Conditions](#) and the [Ethical guidelines](#) still apply. In no event shall the Royal Society of Chemistry be held responsible for any errors or omissions in this *Accepted Manuscript* or any consequences arising from the use of any information it contains.



Journal Name

ARTICLE

## Multiscale Study of Mononuclear Co<sup>II</sup> SMMs based on Curcuminoid Ligands

Received 00th January 20xx,  
Accepted 00th January 20xx

DOI: 10.1039/x0xx00000x

www.rsc.org/

Raúl Díaz-Torres,<sup>a</sup> Melita Menelaou,<sup>a</sup> Olivier Roubeau,<sup>b</sup> Alessandro Sorrenti,<sup>c</sup> Guillem Brandariz-de-Pedro,<sup>a</sup> E. Carolina Sañudo,<sup>a</sup> Simon J. Teat,<sup>d</sup> Jordi Fraxedas,<sup>ef</sup> Eliseo Ruiz<sup>ag</sup> and Núria Aliaga-Alcalde<sup>h\*</sup>

*This work introduces a novel family of Co<sup>II</sup> species having attached a curcuminoid (CCMoid) ligand, 9Accm, namely [Co(9Accm)<sub>2</sub>(py)<sub>2</sub>] (1) and [Co(9Accm)<sub>2</sub>(2,2'-bpy)] (2), achieved in high yields by the use of a microwave reactor, and exhibiting two different arrangements for the 9Accm ligands, described as "cis" (2) and "trans" (1). The study of the similarities/differences of the magnetic, luminescent and surfaces behaviors of the two new species, 1 and 2, is the main objective of the present work. The determined single-crystal structures of both compounds are the only Co<sup>II</sup>-CCMoid structures described in the literature so far. Both compounds exhibit large positive D values, that of 1 (D = +74 cm<sup>-1</sup>) being three times larger than that of 2 (D = +24 cm<sup>-1</sup>), and behave as mononuclear Single-Molecule Magnets (SMMs) in the presence of an external magnetic field. Their similar structures but different anisotropy and SMM characteristics provide, for the first time, deep insight on the spin-orbital effects thanks to the use of CASSCF/NEVPT2 calculations implementing such contributions. Further magnetic studies were performed in solution by means of paramagnetic <sup>1</sup>H NMR, where both compounds (1 and 2) are stable in CDCl<sub>3</sub> and display high symmetry. Paramagnetic NMR appears to be a useful diagnostic tool for the identification of such molecules in solution, where the resonance values found for the methine group (-CH-) of 9Accm vary significantly depending on the cis or trans disposition of the ligands. Fluorescence studies show that both systems display chelation enhancement of quenching (CHEQ) with regards to the free ligand, while 1 and 2 display similar quantum yields. Deposition of 1-2 on HOPG and Si(100) surfaces using spin-coating was studied by AFM; UV photoemission experiments under the same conditions display 2 as the most robust system. The measured occupied density of states of 2 with UV photoemission is in excellent agreement with theoretical DFT calculations.*

### Introduction

Within a variety of frameworks and different time periods, fields like molecular electronics,<sup>1</sup> molecular magnetism<sup>1a,2</sup> and molecular spintronics<sup>2a-c,3</sup> have pointed out the relevance of organic systems and coordination compounds toward their application in

nanoscience and nanotechnology.<sup>1-3,4</sup> For that, the reliable characterization of the performance of such entities not only in the solid state and solution but also on surfaces/devices is mandatory.<sup>5</sup> Small and rather straightforward coordination compounds provide effective solutions allowing clear understanding of their functioning and improving fundamental and applied research. Great efforts are directed toward the design of molecular compounds taking into account the overall effects of the organic ligands and metals attached,<sup>6</sup> task not always easy to anticipate. In the metal-ligand consortium, the former can provide redox, magnetic and/or luminescent properties,<sup>2,7</sup> among others, and tune others like optical performance<sup>8</sup> or luminescence.<sup>9</sup> This together with the power of organic matter of introducing new properties allows suitable functional materials created by the synergy of both. In this sense, mononuclear coordination compounds are gaining relevance as autonomous units that ultimately can function as building blocks<sup>10</sup> in more elaborated structures. To facilitate the correct development of the above mentioned fields, further insight on the factors that affect the final properties is crucial including stability and robustness. Realistic use of molecular materials implies also the study of performance upon deposition on surfaces and<sup>11</sup> among electrodes/inside devices.<sup>1a,12</sup> We direct our efforts to integrate mononuclear functional coordination compounds into the areas described above, by giving relevance to both the metal center and the organic ligands attached

<sup>a</sup> Departament de Química Inorgànica, Universitat de Barcelona, Diagonal 645, 08028 Barcelona, Spain.

<sup>b</sup> Instituto de Ciencia de Materiales de Aragón (ICMA), CSIC and Universidad de Zaragoza, Plaza San Francisco s/n 50009 Zaragoza, Spain.

<sup>c</sup> CSIC-ICMAB (Institut de Ciència dels Materials de Barcelona) Campus de la Universitat Autònoma de Barcelona, 08193 Bellaterra, Spain.

<sup>d</sup> Advanced Light Source, Lawrence Berkeley National Laboratory, Berkeley, California 94720, USA.

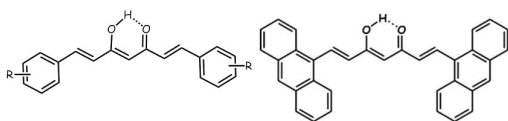
<sup>e</sup> CN2 - Institut Català de Nanociència i Nanotecnologia, Campus UAB, 08193, Bellaterra (Barcelona), Spain.

<sup>f</sup> CSIC - Consejo Superior de Investigaciones Científicas, ICN2 Building, 08193 Bellaterra (Barcelona), Spain.

<sup>g</sup> Institut de Química Teòrica i Computacional, Universitat de Barcelona, Diagonal, 645, 08028 Barcelona, Spain.

<sup>h</sup> ICREA (Institució Catalana de Recerca i Estudis Avançats) & CSIC-ICMAB (Institut de Ciència dels Materials de Barcelona) Campus de la Universitat Autònoma de Barcelona, 08193 Bellaterra, Spain.

† Electronic Supplementary Information (ESI) available: Detailed description of materials and methods, crystallography, physical methods, computational methods, paramagnetic <sup>1</sup>H NMR, UV-Vis, AFM and photoemission. CCDC numbers 1411573 (1) -1411574 (2). See DOI: 10.1039/x0xx00000x



Scheme 1. General drawing of a symmetric CCMoid (left) and the ligand 9Accm (right) in their enol forms, respectively.

to it. The organic groups selected for such enterprise are curcumin derivatives also called curcuminoids (CCMoids), depicted in Scheme 1, left. CCMoids are synthetic bio-inspired molecules well-known in bio-oriented fields<sup>13</sup> recently introduced in molecular magnetism and molecular electronics by some of us.<sup>14-16</sup> In particular, the ligand used in this work, 9Accm (Scheme 1, right),<sup>14</sup> was tested at the nanoscale, behaving as a nanowire capable of electronic transport in carbon-based gateable molecular junctions.<sup>15</sup> Attached to metals, 9Accm has produced complexes with relevant biological, magnetic or visible/near-IR luminescent properties.<sup>9,16</sup> Apart from its fluorescent properties, 9Accm appears to be an excellent platform to contact graphene electrodes or to attach coordination compounds on carbon-based surfaces.<sup>15</sup> We are interested in the study of such affinity applied now to a family of cobalt coordination compounds.

Here, we introduce two novel hexacoordinated Co<sup>II</sup> compounds, [Co(9Accm)<sub>2</sub>(py)<sub>2</sub>] (**1**) and [Co(9Accm)<sub>2</sub>(2,2'-bpy)] (**2**), to the best of our knowledge the only two systems crystallographically described using CCMoid ligands. Compounds **1** and **2** differ in the disposition of the coordinated 9Accm ligands. The present work means to relate the magnetic/fluorescent responses of two Co<sup>II</sup> compounds with the inherent properties that the arrangement of the ligands confers to the final compounds in the bulk, solution and on surfaces. Studies in the solid state show that **1** and **2** present almost identical ligands, do not exhibit highly-distorted coordination environment but clearly differ magnetically due to the tuning of the metal coordination. Insight on spin-orbital effects has been accomplished through theoretical calculations. This thorough analysis includes comparison with the limited family of mononuclear Co<sup>II</sup> hexacoordinated SMMs. Studies of stability of the two systems in solution were targeted by the use of paramagnetic <sup>1</sup>H NMR technique with subsequent fluorescent experiments. To describe the affinity and robustness, deposition of **1** and **2** on HOPG/Si(100) substrates are described together with their analyses by photoemission experiments, corroborated by theoretical studies as well.

## Experimental

Synthesis of [Co(9Accm)<sub>2</sub>(py)<sub>2</sub>] (**1**). The new system was synthesized by adding in a microwave (MW) tube 26 mg of [Co(O<sub>2</sub>CMe)<sub>2</sub>·4H<sub>2</sub>O] (0.104 mmol) together with 100 mg of 9Accm (0.210 mmol) in 5 mL of pyridine, remaining most of the free ligand insoluble. The MW conditions allowed the temperature and pressure to rise freely at

the same time that strong stirring was applied. After less than 2 min the maximum temperature was reached (140 °C) and kept constant during 2 more min. The reaction was then cooled to room temperature, resulting in a clear brown solution from which nice crystals were directly isolated after several hours standing. Yield: 102 mg (83 %). Anal. Calcd. for C<sub>80</sub>H<sub>56</sub>CoN<sub>2</sub>O<sub>4</sub>·0.2C<sub>5</sub>H<sub>5</sub>N (1183.17 g·mol<sup>-1</sup>): C 82.16; H 4.85; N 2.60. Found: C 82.06; H 4.73; N 2.50. IR data (KBr, cm<sup>-1</sup>): 3434(br), 3048(w), 3016(w), 2925(w), 2846(w), 1632(w), 1558(m), 1504(s), 1441(s), 1349(w), 1296(w), 1259 (w), 1212(w) 1162(w), 970(w), 887(w), 734(m), 696(w), 444(w). MALDI<sup>+</sup> (DHB) (m/z): 1010.3 [(Co(9Accm)<sub>2</sub> + H)<sup>+</sup> and 1032.3 [(Co(9Accm)<sub>2</sub> + Na)<sup>+</sup>].

Synthesis of [Co(9Accm)<sub>2</sub>(bpy)] (**2**). Compound **2** was obtained using identical MW parameters as before, and adding 26 mg of [Co(O<sub>2</sub>CMe)<sub>2</sub>·4H<sub>2</sub>O] (0.104 mmol), 100 mg of 9Accm (0.210 mmol) and 16 mg of 2,2'-bipyridine (0.102 mmol) to a MW tube using 5 mL of DMF as solvent. Yield: 107 mg (88 %). Crystals suitable for analyses were achieved by slow evaporation of the final solid in CHCl<sub>3</sub>. Anal. Calcd. for C<sub>80</sub>H<sub>54</sub>CoN<sub>2</sub>O<sub>4</sub>·0.2 C<sub>3</sub>H<sub>7</sub>NO (1179.95 g·mol<sup>-1</sup>): C 81.98; H 4.73; N 2.61. Found: C 81.83; H 4.63; N 2.48. IR data (KBr, cm<sup>-1</sup>): 3429(br), 3043(w), 3021(w), 2994(w), 2917(w), 2848(w), 2087(w), 1672(m), 1630(m), 1598(w), 1551(m), 1506(s), 1442(m), 1351(m), 1311(w), 1264(w), 1161(m), 1017(w), 968(m), 879(m), 842(w), 763(m), 733(s), 602(w), 540(w), 446(w). MALDI<sup>+</sup> (DHB) (m/z): 690.1 [(Co(9Accm)(2,2'-bpy))<sup>+</sup> and 1032.3 [(Co(9Accm)<sub>2</sub> + Na)<sup>+</sup>].

## Results and discussion

### Synthesis

Compound **1** [Co(9Accm)<sub>2</sub>(py)<sub>2</sub>], and **2**, [Co(9Accm)<sub>2</sub>(2,2'-bpy)], were synthesized using a microwave (MW) reactor. This methodology, well-established for organic molecules,<sup>17</sup> has been also described in the past for the achievement of coordination compounds<sup>17</sup> and used by some of us in related compounds to those described here.<sup>16a</sup> In our experience, microwave assisted technique has improved yields and allowed the increase of amount of starting materials used, decreasing drastically the volume of the required solvents together with reaction times.<sup>16a,17,18</sup> In the case of pyridine (compound **1**), crystals were obtained directly from the microwave tube after cooling down the reaction. Here, the presence of pyridine or 2,2'-bipyridine is the key factor for the reorganization of the 9Accm around the Co<sup>II</sup> centers and therefore, responsible of the differences between **1** and **2**.

### Structural Descriptions

Compounds **1** and **2** are the first Co-CCMoids crystallographically described in the literature so far.

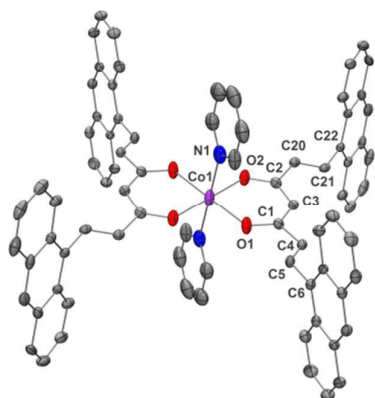


Fig 1. POV-Ray view of **1** with thermal ellipsoids fixed at 30 %. Protons are omitted for the sake of simplification. Color legend: Co in magenta, O in red, N in blue and C in grey.

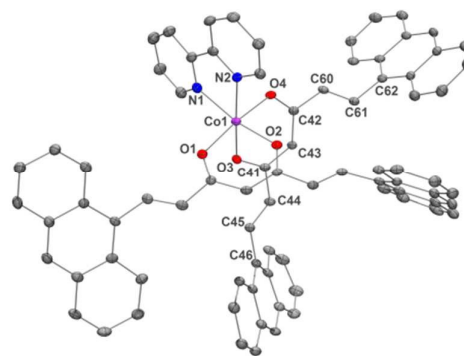


Fig 2. POV-Ray view of **2** with thermal ellipsoids fixed at 50 %. Protons as well as the lattice chloroform molecule are omitted for clarity. Color legend: Co in magenta, O in red, N in blue and C in grey.

General crystal data information of the two species is presented in Table S1. Compound **1**, [Co(9Accm)(py)<sub>2</sub>], crystallizes in the monoclinic space group  $P2_1/c$ . The mononuclear species contain one hexacoordinated Co<sup>II</sup> centre that binds two molecules of 9Accm and two molecules of pyridine. The organic pairs of ligands display a *trans* conformation providing a  $D_{4h}$  ideal geometry. Selected bond lengths and angles are listed in Table S1 and Figure 1 shows a POV-Ray projection for compound **1**. This molecule shows two Co-O distances of 2.002(2) and 2.033(2) Å and one Co-N distance of 2.209(4) Å, in agreement with others reported elsewhere.<sup>19</sup> O(1)-Co-O(2') and O(1)-Co-O(2) angles are of 89.88 and 90.13 °, respectively, while O(1)-Co-O(1'), O(2)-Co-O(2') and N(1)-Co-N(1') are all 180 ° by symmetry. Basically, the coordinated 9Accm ligands display two alternating C-C values: C(1)-C(4), C(5)-C(6), C(2)-C(20) and C(21)-C(22) relate to single C-C distances (1.400-1.486 Å) and on the other hand, C(4)-C(5) and C(20)-C(21) show characteristic double C-C bonds (between 1.311 and 1.315 Å). Such distances are found in related compounds.<sup>14,16</sup> It must be stressed that the conjugated chains in the two sides of the ligand have a different conformation, either zig-zag or boat shape, emphasizing the flexibility of the organic molecule and the diversity on its packing by comparing with the free ligand and reported compounds.<sup>14,16</sup> No relevant hydrogen bonds or  $\pi$ -stacking interactions are found in the structure, with the shortest Co<sup>II</sup>...Co<sup>II</sup> distance at 8.962 Å.

Compound **2**, [Co(9Accm)(2,2'-bpy)], crystallizes in the monoclinic space group  $P2_1/n$ . The structure shows a similar compound as **1**, with a Co<sup>II</sup> center bound to two molecules of 9Accm disposed in a *cis* arrangement and one molecule of 2,2'-bipyridine, now resulting in a  $C_{2v}$  ideal symmetry. The Co-O distances between 2.012 and 2.071 Å and Co-N between 2.109 and 2.115 Å, respectively, related to others in the literature.<sup>19</sup> On the contrary, O-Co-O, N-Co-N and O-Co-N angles differ slightly with respect to **1** (see Table S3). Similar

values as in the structure of **1** are found for the C-C distances in both 9Accm ligands, with one of them presenting its two sides in zig-zag conformation meanwhile the other shows zig-zag and boat-shape conformations. The shortest Co<sup>II</sup>...Co<sup>II</sup> separation is of 10.105 Å and no significant supramolecular interactions can be identified, except a short C-H...O contact of the lattice chloroform molecule with O3, at 2.269 Å.

Both crystal structures could only be achieved by the use of X-ray synchrotron source. The flexibility of the chain observed in **1** and **2** by the different arrangements and the absence of further supramolecular interactions among neighbouring molecules could be associated to the small size of the crystals and the difficulties, observed also in related coordination compounds, of growing them.

### Studies in Solution

#### Paramagnetic proton NMR

<sup>1</sup>H NMR of **1** and **2** were measured in CDCl<sub>3</sub> and shown in Figure 3. Contrary to most of paramagnetic nuclei, octahedral (*Oh*) Co<sup>II</sup> centers display slow nuclear relaxation.<sup>20</sup> Therefore, spectral features of "[Co(9Accm)<sub>2</sub>]" systems are found sharp enough to use NMR as a diagnostic tool for their analyses in solution.<sup>20</sup> To gain further insight on the paramagnetic features of **1** and **2**, their stability in solution and the effect of geometry, additional *cis* and *trans* compounds (**3** - **6**) were synthesized and characterized by IR, EA and ESI (SI). Hence, two additional *trans* compounds with formulae [Co(9Accm)<sub>2</sub>(3,5-(CH<sub>3</sub>)<sub>2</sub>-py)<sub>2</sub>] (**3**) and [Co(9Accm)<sub>2</sub>(dmf)<sub>2</sub>] (**4**), together with two *cis* compounds, [Co(9Accm)<sub>2</sub>(4,4'-(CH<sub>3</sub>)<sub>2</sub>-2,2'-bpy)] (**5**), and [Co(9Accm)<sub>2</sub>(5,5'-(CH<sub>3</sub>)<sub>2</sub>-2,2'-bpy)] (**6**) were studied in solution gathering information about the nature of most of the peaks. In addition, the available literature on mononuclear Co<sup>II</sup> systems containing pyridinic and acac groups was of great relevance for the assignment of peaks.<sup>21</sup>

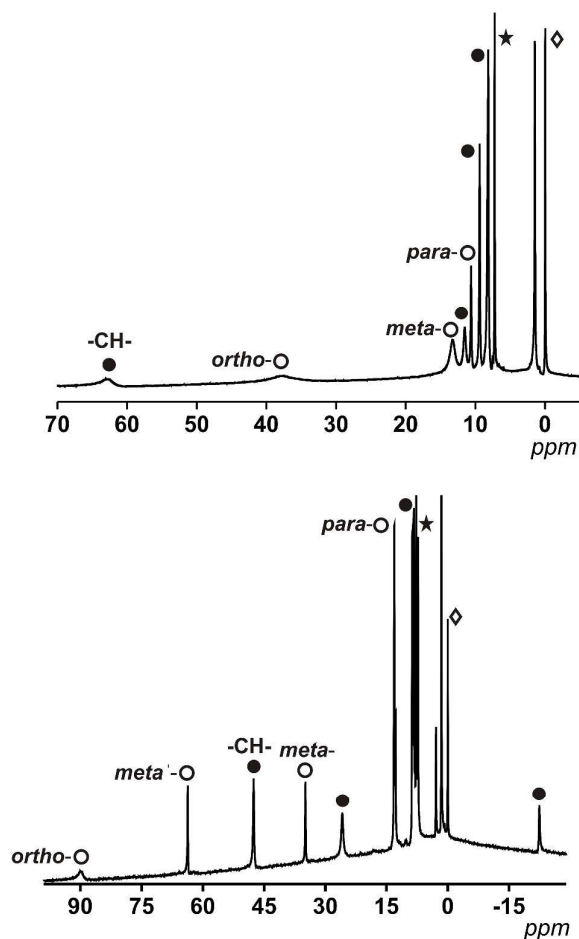


**Fig 3.** a)  $^1\text{H}$  NMR spectrum of **1** in  $\text{CDCl}_3$  between 5–70 ppm. b):  $^1\text{H}$  NMR spectrum of **2** in  $\text{CDCl}_3$  between 30–100 ppm. White spheres relate to protons from py (a) or 2,2'-bpy (b) and black spheres to coordinated 9Accm, respectively. \* $\text{CDCl}_3$  and  $^0\text{TMS}$ .

For **1**, that displays an ideal  $D_{4h}$  symmetry, the number of peaks in the proton NMR reduces to eight (taking into account the overlap of some of the signals, free rotation of the anthracene groups in solution and fast conformations that the 9Accm chain can experience), as if there was only one magnetically unique 9Accm and pyridine ligand as well. As Figure 3a shows, compound **1** presents two distinct regions in a window of approximately 75 ppm: (i) two broad resonances in the downfield area (38 and 63 ppm, respectively) and (ii) six sharper shifts that vary on intensity between 15 and 0 ppm (upfield). The position and shape of the downfield signals relate to the closest protons to the  $\text{Co}^{\text{II}}$  center, being these: the methine -CH- from the 9Accm groups and the ones in *ortho*- from the two pyridine molecules.<sup>22</sup> The assignments of these two signals were based on previous literature<sup>21</sup> and the comparison between **1** and compounds **3** and **4** (Figures S1 and S2, respectively).

From the data collected, the peak at 63 ppm was assigned to the -CH- of 9Accm appearing in all three compounds; meanwhile, the

absence of the broad peak at 38 ppm in **4** proved a pyridinic origin. The latest together with two other sharper peaks at 12.1 and 8.0 ppm were related to the *ortho*-, *para*- and *meta*- protons of the pyridine molecule, respectively. The general appearance and order of proton shifts for the coordinated py molecules suggest contact shifts via  $\pi$  delocalization as the major contributor.<sup>23</sup> The rest of signals of the upfield sector ( $\sim 10$  to 0 ppm) were associated to the chain and anthracene groups from the 9Accm ligands, further away from the metallic nuclei and therefore less affected.<sup>21–24</sup> The individual assignment of the latest could not be made however, the spectrum is consistent with the retention of the idealized symmetry of **1** in solution. The complete list of peaks for **1**, **3** and **4** is shown in Table S2.

Figure 3b shows the spectrum of **2**. The ideal symmetry of this system ( $C_{2v}$ ) would make the two halves of the 2,2'-bpy molecule and the two 9Accm ligands equivalent. The experiment shows that the spectrum comes close to the expected displaying one type of 9Accm and four signals for the 2,2'-bpy (*ortho*-, *meta*-, *meta'*- and *para*- protons). Earlier publications on the subject<sup>21,24</sup> together with comparison of **2** and compounds **5** and **6** has allowed the assignments of the peaks. Now, the system presents a richer downfield area exhibiting sharp resonances at 89.1, 63.0, 47.0, 34.6 and 25.7 ppm with an upfield region that goes from 13.0 to -22.3 ppm. Table S3 shows the list of resonances for **2**, **5** and **6** and Figures S3 and S4 the spectra of **5** and **6**, respectively.

Previous literature shows an usual *ortho*-, *meta'*-, *meta*- and *para*- order (from downfield to upfield) for the proton resonances in  $\text{Co}^{\text{II}}$ - (2,2'-bpy) systems. Also, former compounds showed shifts comparable to those found for compound **2**.<sup>21,22</sup> This, together with the study of **5** and **6** allow the assessment of the two downfield shifts, at  $\sim 90$  and 63 ppm, that correspond to the *ortho*- and *meta'*- protons from the 2,2'-bpy. The following resonance at 47 ppm relates to the methine -CH- proton of the 9Accm, drastically shifted comparing with compound **1** (which appears at 63 ppm). The following *meta*- and *para*- shifts from the 2,2'-bpy were assigned at  $\sim 35$  and  $\sim 13$  ppm, respectively, being the rest of signals ( $\sim 26$ ,  $\sim 13$ , 8.7–7.7 and -22 ppm) of CCMoid nature (chain and anthracene groups of coordinated 9Accm) as it is indicated in Figure 3b.

Overall, the NMR studies of **1** and **2** provide information about (i) the preservation of the molecular structures in solution, (ii) the flexibility of the chain in 9Accm and fast free rotations of anthracene groups and (iii) the great influence of the paramagnetic center on the ligands upon coordination clearly shown by the shift between the methine peaks (-CH-) of **1** and **2** (16 ppm of difference) and the display of resonances of curcuminoid nature at the highest fields present in **2** (-22 ppm). In addition, thanks to the information gathered, paramagnetic  $^1\text{H}$  NMR can be used to predict the *cis* or *trans* nature of future “[ $\text{Co}(\text{CCMoid})_2$ ]” systems by the evaluation of the shift of the -CH- from the coordinated CCMoid.

#### UV-Vis absorption spectra and Fluorescence

The electronic spectra of **1** and **2** in distilled THF showed absorptions around 255 and 425 nm band regions (Figure S5). Intense bands were observed at the highest energies, related to  $\pi$ -

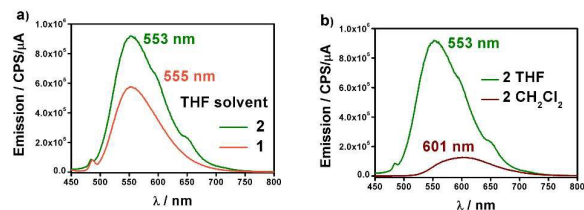


**Fig 4.** (a) Emission spectra of **1** (orange) and **2** (green) in distilled THF. (b) Emission spectra of **2** in distilled  $\text{CH}_2\text{Cl}_2$  (brown) and THF (green).

$\pi^*$  transitions.<sup>9,16c</sup> Smaller broad bands, with maxima at 426 and 424 nm for **1** and **2**, respectively, were associated to the CCMoid character ( $\pi-\pi^*$ ) of both systems, with small hypsochromic shifts for both, **1** and **2**, compared with the free ligand, 9Accm (427 nm), due to the coordination to the metal centers.<sup>14,16</sup> A shoulder between 300-400 nm is sometimes appreciable with maxima features characteristic to anthracene groups. In  $\text{CH}_2\text{Cl}_2$ , the lowest energy bands appeared now at 437 (**1**) and 428 (**2**) nm, indicating higher solvatochromic effects for **1** than **2** (Figure S6).<sup>16c</sup>

Figure 4a shows the fluorescence emission spectra of **1** and **2** in distilled THF when excited at 426 and 424 nm, respectively. Fluorescence band values were found of 555 and 553 nm, in that order. The observed shifts are very close to the free 9Accm ( $\lambda_{\text{em,max}} = 555$  nm), displaying similar behaviours. The shape and large Stokes shift of the bands show the CCMoid origin of the fluorescence as well as suggest small changes in the molecules following excitation most likely due to loss of symmetry or aggregation status.<sup>9,16a,c</sup>

The quantum yields of the two compounds are in sharp contrast to those of ligand 9Accm, which exhibited stronger fluorescence emission (Figure S7). This fact is common in paramagnetic metal centers that normally act as quenchers displaying chelation enhancement of quenching (CHEQ) effects.<sup>9,25</sup> Despite that, both  $[\text{Co}(\text{9Accm})_2]$  systems depict reasonable emissions most likely due to the number of anthracene groups per molecule, their free rotation in solution and the relatively long distance between such groups and the  $\text{Co}^{\text{II}}$ . The emission intensity of **1** is slightly smaller than **2**, fact that is reflected in their quantum yield values,  $\phi$ , being 0.0010 and 0.0014 for compounds **1** and **2**, respectively; both,

approximately, one order of magnitude smaller than the free 9Accm (0.010).<sup>14</sup>

The solvatochromic properties were explored by recording their emission spectra in  $\text{CH}_2\text{Cl}_2$  and comparing with those published for free 9Accm. Figure 4b shows as example, the results for compound **2**. The first observation is that emission intensities are significantly higher in THF than in  $\text{CH}_2\text{Cl}_2$ , indicating additional quenching effect of the latest. In addition, there is a bathochromic effect (red shift) of  $\sim 50$  nm, from THF (555 (**1**) and 553 (**2**) nm) to  $\text{CH}_2\text{Cl}_2$  appearing now the maxima at 603 and 601 nm for both compounds (Figures S8 and 4b), respectively, and significantly shifted ( $\sim 25$  nm) from the free ligand under the same conditions (577 nm).<sup>16c</sup> The results show solvatochromic emissions for **1** (Figure S8) and **2** (Figure 4b) in a similar way than others published in the past as well as the effect of solvent polarity on the final emissions.<sup>16b,c</sup> Overall, fluorescence is qualitatively affected in the same manner for both compounds.

### Solid State Properties

#### Static Magnetic Properties

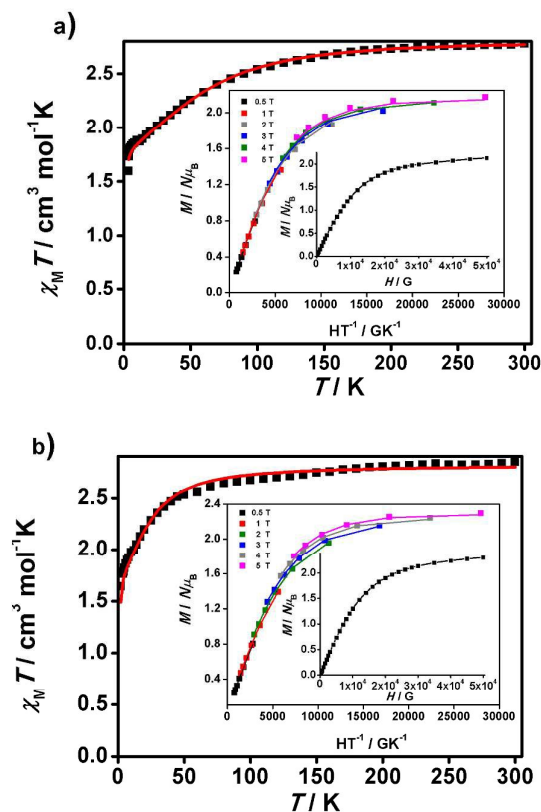


**Fig 5.**  $\chi_M T$  vs.  $T$  graphs and insets,  $M/N\mu_B$  vs.  $H/T$  and  $M/N\mu_B$  vs.  $H$  data, for **1** (a) and **2** (b), respectively. Experimental data are shown as dots and the resulting fitting as a line.

**Table 1.**  $\phi$  stands for quantum yield. Values of  $D$  and  $E$  (all in  $\text{cm}^{-1}$ ) for the  $S = 3/2$  ground state of compounds **1** and **2** calculated with CASSCF and NEVPT2 (values in parenthesis) methods (see Computational details section). The last two columns give the first excitation energy  $\delta$  and  $\Delta$  (in  $\text{cm}^{-1}$ ) without and after including spin-orbit effects, respectively. The  $\Delta$  value corresponds to the energy difference between the ground and excited Kramers' doublets.

	$\phi$	$D_{\text{fitting}}$	$E_{\text{fitting}}$	$g_{\text{fitting}}$	$D_{\text{calc}}$	$E_{\text{calc}}$	$\delta_{\text{calc}}$	$\Delta_{\text{calc}}$
<b>1</b>	0.0010	74.1	1.21	2.26	167.1 (146.5)	24.0 (25.6)	405 (463)	227 (214)
<b>2</b>	0.0014	24.1	-1.89	2.39	71.6 (50.2)	7.8 (6.8)	775 (1095)	152 (113)

Lately a fast growing family of mononuclear  $\text{Co}^{\text{II}}$  SMMs have been described<sup>26</sup> and some of us have incorporated straightforward rules to identify them.<sup>27</sup> Compounds **1** and **2** follow the requirements as possible SMM candidates and therefore magnetic susceptibility were measured on polycrystalline samples of **1** and **2** using *dc* and *ac* techniques. Herein, the *dc* magnetic studies are presented as  $\chi_{\text{M}}T$  vs.  $T$ ,  $M/N\mu_{\text{B}}$  vs.  $H$  and  $M/N\mu_{\text{B}}$  vs.  $H/T$  plots (Figure 5),  $\chi_{\text{M}}$  being the molar paramagnetic susceptibility and  $N$  and  $\mu_{\text{B}}$  having the usual meaning. The temperature dependences of the  $\chi_{\text{M}}T$  product of **1** and **2** are displayed in Figures 5a and 5b, together with their  $M/N\mu_{\text{B}}$  vs.  $H$  plots (insets). At 300 K, the  $\chi_{\text{M}}T$  products of **1** and **2** are equal to 2.77 and 2.87  $\text{cm}^3 \text{K mol}^{-1}$ , respectively, both higher than calculated for an isolated  $S = 3/2$  system ( $\chi_{\text{M}}T = 1.875 \text{ cm}^3 \text{K mol}^{-1}$ ,  $g = 2.0$ ) due to expected spin-orbital contributions. Lowering the temperature, the  $\chi_{\text{M}}T$  products are smoothly decreasing down to respectively 100 K and 50 K, before dropping in a smooth way for **1** to reach 1.59  $\text{cm}^3 \text{K mol}^{-1}$  at 3 K and more abruptly for **2**, reaching the value of 1.64  $\text{cm}^3 \text{K mol}^{-1}$ , at 2 K. In addition,  $M$  vs.  $H/T$  data were collected in the magnetic field-temperatures range of 0.5 - 5 T and 1.8 - 6.8 K to determine the zero-field splitting and rhombic parameters ( $D$  and  $E$ ) for both compounds, respectively. The resulting data for **1** and **2** are plotted in Figure 5 (inset) as reduced magnetization  $M/N\mu_{\text{B}}$  vs.  $H/T$ . The data were fit by diagonalization of the spin Hamiltonian matrix, using the program PHI,<sup>28</sup> which allows the correlation of experimental magnetic data of orbitally degenerate systems using multiple sources; in this case,  $\chi_{\text{M}}T$  vs.  $T$  data together with  $M$  vs.  $H/T$  results were used simultaneously. The obtained fit gave  $g = 2.26$ ,  $D = 74.1 \text{ cm}^{-1}$  and  $E = 1.21 \text{ cm}^{-1}$  for **1** and  $g = 2.39$ ,  $D = 24.1 \text{ cm}^{-1}$  and  $E = -1.89 \text{ cm}^{-1}$  for **2** (Figures 5a and 5b). Large  $D$  values were already expected from the analysis of the  $M/N\mu_{\text{B}}$  vs.  $H$  data at 2 K, that presents saturation at the highest magnetic fields (population of the lowest  $m_s$  state) for **1** and **2**, with values close to 2  $\mu_{\text{B}}$  (2.13 and 2.28  $\mu_{\text{B}}$ , respectively), lower than those expected for a  $S = 3/2$  ( $M/N\mu_{\text{B}} = 3.0 \mu_{\text{B}}$ ,  $g = 2$ ), indicating that there are considerable orbital contributions in both cases. Indeed, the  $D$  value of **1** is comparable to the highest  $D$  value of 80  $\text{cm}^{-1}$  described until now by Cano *et al.*<sup>26h</sup>

Further analyses of the second-order anisotropy parameters (value and sign of  $D$  and  $E$ ) were pursued based on Eqs 1, 2 and 3<sup>29</sup> being both anisotropic parameters derived from the principal elements of the  $D$  tensor

$$D = D_{zz} - \frac{D_{xx} + D_{yy}}{2} \quad (1)$$

$$E = \frac{D_{xx} - D_{yy}}{2} \quad (2)$$

that can be estimated as follows:

$$D_{kl} = -\frac{\zeta_{\text{eff}}^2}{4S^2} \sum_{i,p} \frac{\langle \varphi_i | l_k | \varphi_p \rangle \langle \varphi_p | l_l | \varphi_i \rangle}{\varepsilon_p - \varepsilon_i} - \frac{\zeta_{\text{eff}}^2}{4S^2} \sum_{p,a} \frac{\langle \varphi_p | l_k | \varphi_a \rangle \langle \varphi_a | l_l | \varphi_p \rangle}{\varepsilon_a - \varepsilon_p} \quad (3)$$

where  $\zeta_{\text{eff}}$  is the monoatomic spin-orbit coupling constant;  $l_x, l_y, l_z$  are the  $x, y, z$  components of the angular momentum operator, and  $\varepsilon_i$  the molecular orbital energies with the sub-index  $i, p$  or  $a$ , that indicate double-occupied, singly-occupied or empty orbitals, respectively. Intuitively, following Eq 3, small excitation energies ( $\delta$  in Table 1) results also in orbital energies differences give rise to large diagonalized  $D_{ij}$  values ( $\delta \approx \varepsilon_p - \varepsilon_i$  and  $D_{ii} = D_{xx}, D_{yy}$  or  $D_{zz}$ ).<sup>27</sup> In the case of a single  $\text{Co}^{\text{II}}$  ion ( $d^7$ ) in a pseudo-octahedral coordination with  $d_{xz}^2, d_{yz}^2, d_{xy}^1, d_{z^2}^1, d_{x^2-y^2}^1$  orbital occupation (like **1** and **2**), the first excitation energies,  $\delta$ , correspond to transitions between the beta  $d_{xz}$  or  $d_{yz}$  orbitals and the beta  $d_{xy}$  orbital, which are small (see Table 1), explaining the high values of  $D$  for both compounds (where **1** is one of the highest found in literature). On the other hand, **1** and **2** are described as easy-plane systems instead of being easy-axis taking into account the above excitation energies, the symmetry of the orbitals involved (change absolute  $m_l$  value in the first excitation) and the fact that the operator matrix  $D_{xx}$  and  $D_{yy}$  terms are predominant.<sup>30</sup> Thus, the  $(D_{xx} + D_{yy})/2$  term in Eq 1 will be larger than the  $D_{zz}$  term, resulting in positive  $D$  values (all terms of Eq 3 are strictly negative). These qualitative arguments have been confirmed by CASSCF/NEVPT2 calculations including spin orbit effects (Table 1) agreeing with the positive signs and large values of  $D$  found in the fittings of **1** and **2**, respectively.

### Dynamic Magnetic Properties

The *ac* magnetic susceptibility of **1** and **2** below 5 K was investigated under the presence of external *dc* fields, as no out-of-phase signals were observed in zero-field. Experiments at variable frequency up to 1480 Hz were first performed at different magnetic fields (0.05, 0.1, 0.15, 0.2 and 0.5 T for **1** and 0.03, 0.05, 0.07 and 0.1 T, in the case of **2**) to determine the most convenient *dc* field for the study of the magnetization dynamics of each compound. Figures S9 and S10 show the resulting  $\chi''_{\text{M}}$  vs. frequency plots, in which a maximum is observed at all fields in the case of **1**, while only at the higher fields and close to the maximum frequency in the case of **2**.

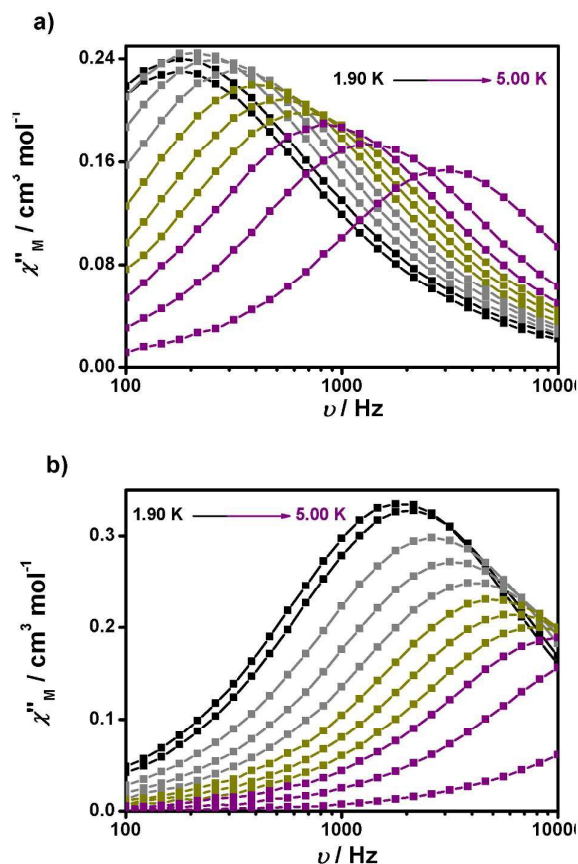


**Fig 6.** Frequency dependence of the out-of-phase ( $\chi''_M$  vs.  $\nu$ ) susceptibility for **1** (a) and **2** (b) under 1500 and 700 Oe *dc* fields, respectively.

The optimal fields were defined as 0.15 and 0.07 T respectively for **1** and **2**.

Experiments at variable frequency were then repeated in the extended 100 Hz to 10 kHz range at these *dc* field and temperatures in the range 1.9 to 6 K. The characteristic frequency dependence of the in-phase ( $\chi'_M$ ) and out-of-phase ( $\chi''_M$ ) susceptibilities for a SMM behaviour is clearly observed in both cases (Figures 6a and 6b, respectively, as well as Figures S11 and S12).

From the above experiments, Cole-Cole diagrams were extracted at the same temperature range (Figures 7a and 7b), exhibiting typical semi-circular shapes. These data were fit to the Cole-Cole expressions using C-Cfit program,<sup>31</sup> affording values of the characteristic relaxation time  $\tau$  in the range 0.01–0.20  $\text{s}^{-1}$  for **1** and 0.01–0.30  $\text{s}^{-1}$  for **2**, supporting the existence of a single relaxation process in each case.

From here, the spin-lattice relaxation rate  $\tau^{-1}$  was determined at each given temperature. The complete modelling of it, that is to say dependence  $\tau^{-1}$  vs.  $T$ , can be performed following Eq. 4.<sup>32</sup>

$$\tau^{-1} = AH^2T + \frac{B_1}{1+B_2H^2} + CT^n + \tau_0^{-1}\exp\left(-\frac{U_{\text{eff}}}{kT}\right) \quad (4)$$

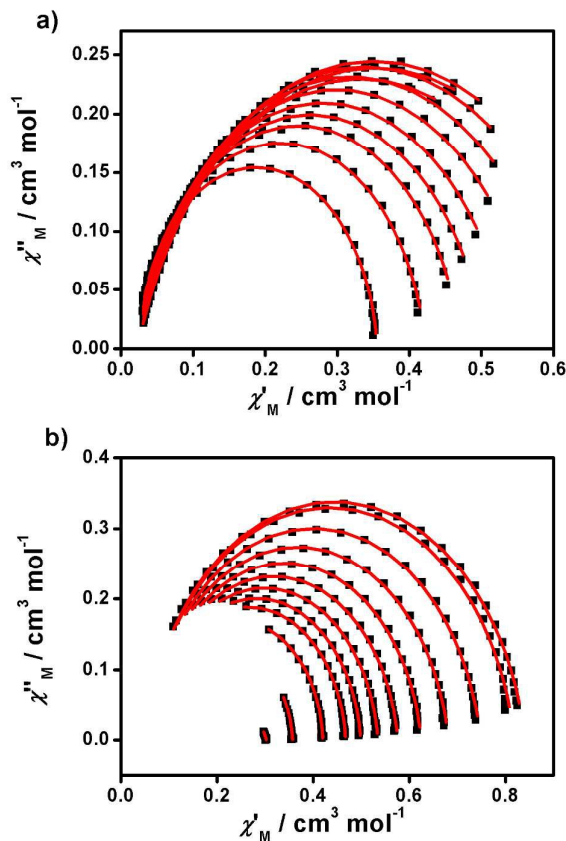


**Fig 7.** Cole-Cole plots of **1** (a) and **2** (b) measured from 1.9 to 5.0 K under 1500 and 700 Oe *dc* fields, respectively.

The terms in Eq. 4 refer to direct relaxation, quantum tunnelling, Raman and Orbach relaxation mechanisms, in that order. Quantum tunnelling contribution are not relevant<sup>26c</sup> and Orbach processes are not considered because the ab initio calculations indicate that the first excited state are much higher in energy than the measured barrier. Hence, Raman and direct relaxation mechanisms were the only two expressions used in the simulation (Eq 5).

$$\tau^{-1} \approx A'T + CT^n \quad (5)$$

The simulated data using Eq. 5 is shown in Figure 8. The extracted  $A'$ ,  $C$  and  $n$  values are depicted in Table 1. To provide further analysis and with the aim of introducing a library of novel magnetic parameters, comparison of these data with published ones for other 3d mononuclear  $\text{Co}^{\text{II}}$  SMMs (Table S4) shows that the  $A'$  value for **1** (447  $\text{s}^{-1} \text{k}^{-1}$  at 0.15T) is comparable to previously derived values<sup>32,33</sup> although the value for **2** (6688  $\text{s}^{-1} \text{k}^{-1}$  at 0.15 T) is one order of magnitude higher than the available data until now.

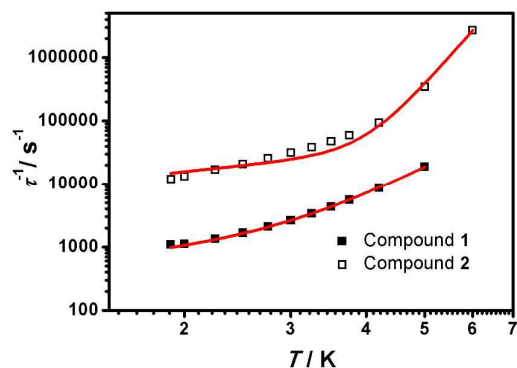


**Fig 8.**  $\tau^{-1}$  vs.  $T$  plots of **1** (■) and **2** (□) measured from 1.9 to 5.0 K under 1500 and 700 Oe *dc* fields, respectively.

Nonetheless, the comparison and interpretation of  $A'$  are not trivial, depending on several parameters,<sup>32</sup> where the scarce information available restrict further conclusions. The case of the Raman term is similar, where we conclude that the  $C$  values found for **1** and **2** are similar to published  $\text{Fe}^{\text{II}}$  systems<sup>32</sup> and again, the highest in contrast with the other  $\text{Co}^{\text{II}}$  SMM studied this way in the literature.<sup>26c</sup> However, here the effect of solid dilution may play a relevant role and therefore numbers should be evaluated with caution. Our  $n$  factors, on the other hand, are of the order of others, being 5 for **1** and 7.5 for **2**,<sup>32,33</sup> and reinforcing the idea that direct and Raman mechanisms are operative. Here again, the appreciable magnetic differences between the two compounds, **1** and **2**, should be highlighted, even though they share similar ligand environment.

### Theoretical results

Calculated second-order anisotropy parameters and excitation energies for compounds **1** and **2** are collected in Table 1. The calculated  $D$  and  $E$  values are in qualitative agreement with the fitted values showing large positive  $D$  values for both compounds, three times larger in the case of **1**. It is usual to expect larger calculated values in comparison with the fitted experimental data, because such spin relaxation mechanisms depending of the lattice effects are not considered in single-molecule calculations. These facts (sign and dimension of  $D$ ) relate to the Jahn-Teller effect that causes distortions breaking the orbital degeneracy (assuming a perfect  $Oh$  coordination) where, as explained above, small energy differences between ground and first excited state ( $\delta$ ) affect  $D$  in great manner, reflected as small denominator values in Eq. 3. The small value of such energy gaps contribute to the uncertainty determining  $D$  (thus, the energy gap,  $\delta$ , is so small that the systems are close to a degenerate ground state) making then first-order spin-orbit contributions also relevant.<sup>27,34</sup> Also previously noticed CASSCF-type calculations generally overestimates  $D$  values, perhaps also caused by the mentioned limitations of the spin Hamiltonian for a near-degenerate system and the lack of inclusion of some spin polarization mechanism (tunneling and collective effects) in the calculations.<sup>27</sup>

The origin of the large anisotropy in first-row mononuclear transition metal complexes is the presence of low-lying spin-orbit free excited states (CASSCF/NEVPT2 energies without spin-orbit contributions,  $\delta$  in Table 1) with close energies to the ground state. Thus, systems showing a distorted geometry (in this case, pseudo-octahedral) due to the Jahn-Teller effect with respect to an ideal degenerate  $d^7$  octahedral configuration are perfect candidates to have close low-lying excited states.

As mentioned above using as model a simple single-determinant wavefunction, the first excitation energies should correspond then to transitions from the beta  $d_{xz}$  or  $d_{yz}$  orbitals to the beta  $d_{xy}$  orbital that would degenerate in the octahedral symmetry ( $t_{2g}$ ). This fact results in large contributions to the  $D$  value (see  $\delta$ , Table 1) although they must be corrected by including first-order spin-orbit contributions (see  $\Delta$ , Table 1). Indeed, by doing so, it is clear why compound **2** displays the largest excitation energy  $\delta$  but the smallest  $D$  value comparing with **1** ( $\Delta$  value is smaller for **2**, see Table 1). Therefore, a reliable orbital explanation for the differences in the  $D$  values of **1** and **2** must include the relative energies of the non-degenerate orbitals ( $d_{xz}$ ,  $d_{yz}$  and  $d_{xy}$ ) taking into account geometrical distortions and the presence of two different ligands (py/9Accm (**1**) and 2,2'-bpy/9Accm (**2**)). Nevertheless, basic qualitative explanations are not trivial, because the orbitals energies are controlled by subtle interplay of many parameters (different metal-ligand distances and ligand-metal-ligand angles for the two types of ligands). Thus, our DFT studies (see details in Photoemission section) show that for **1**, a small splitting of the three orbitals was obtained with the  $d_{xy}$  orbital displaced to the intermediate position among the  $t_{2g}$  orbitals meanwhile in **2**, a larger splitting was found with the  $d_{xy}$  orbital positioned at the highest energy. All together, such variations agree with the values from the fitting and explain the difference between **1** and **2**.

### AFM deposition studies

AFM experiments were performed with deposits of **1** and **2** on highly oriented pyrolytic graphite (HOPG) and silica (Si(100)) surfaces. The experiments were performed with a double aim: the study of their affinity with the above mentioned surfaces and information on their stability from later photoemission experiments. Spin-coating experiments using  $\text{CH}_2\text{Cl}_2$  solutions of **1** and **2** were performed using both substrates, HOPG and Si(100). Blanks using exclusively the solvent at the same conditions were performed for each experiment (Figure S13).

Depositions on freshly cleaved highly oriented pyrolytic graphite (HOPG) were performed at 500 rpm during 30 seconds; three drops of the solutions were added to the surface at regular intervals (~10 s). The HOPG experiments display the affinity of **1** and **2** for such surface due to the  $\pi$ - $\pi$  interactions of the anthracene groups with the substrate at room temperature.<sup>35</sup> At  $10^{-4}$  M, AFM images show the formation of multiple aggregates of molecules with heights between 1.0-1.2 nm for **1** and 1.2-1.6 nm for **2**, respectively (Figures S14 and S15), with average heights corresponding to piles of 1-2 molecules for **1** and **2** on the HOPG surfaces (values estimated from the crystallographic data).

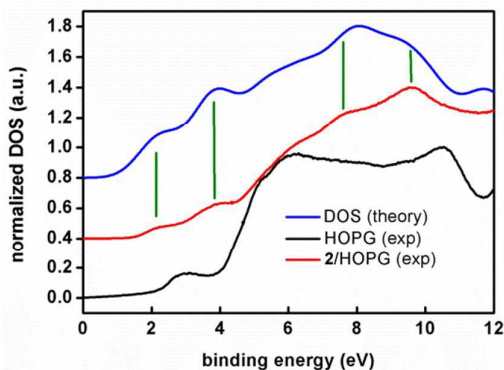


**Fig 9.** Experimental UPS (Ultra-violet Photo-emission Spectroscopy) density of states spectra of a spin-coated film of **2** on HOPG (red) and of a freshly cleaved HOPG surface (black) compared to the DFT calculated (blue). The high-resolution UPS spectra were acquired with pass energy of 5 eV in UHV and at room temperature. Binding energies are referred to the Fermi level of the system ( $E_F = 0$  eV). Spectra have been normalized to their maxima and shifted in the vertical scale for clarity. The DFT calculated DOS spectrum has been shifted by 3.1 eV in order to level the HOMO. Vertical green lines have been included to guide the eye comparing experimental and calculated bands.

Due to the closeness of the aggregates, further experiments were performed to clarify the formation of layer(s) underneath such assemblies. After obtaining an AFM image in tapping mode, the operation was changed to contact mode for both molecules. As we described in the past,<sup>16b</sup> the AFM tip swept the molecules from the substrate due to the higher vertical force applied in contact mode. Afterward, the topographic mode was back to tapping mode and a larger scale was chosen in order to image the area where molecules were removed (Figure S16). The difference between the vertical size on the side of the hole and the undisturbed layer, on the other side, provides great information on the formation of layer(s) and heights. Such experiments were successfully carried out for **2** as is shown in Figure S16. The collected data were similar to the ones described before, indicating the absence of multilayers on the surface of the HOPG substrate. All the attempts to gather the same information with compound **1** failed and final images were vague to provide clear pictures of the surfaces. Toward photoemission experiments, full cover of the surface was accomplished by increasing the number of solution drops of **1** and **2**, respectively, on the HOPG surfaces.

Similar experiments using Si(100) presented clear aggregation even at higher concentrations, being impossible to accomplish full coverage of the surface and therefore further photoemission experiments. Such behaviour directly relates with solvent evaporation effects ( $\text{CH}_2\text{Cl}_2$ ), the conjugated nature of the two compounds and probably the deposition methodology, emphasizing once again the higher affinity of the compounds toward the HOPG.

### Photoemission

XPS experiments on a film of **2** spin-coated on HOPG allowed the identification of spin-orbit splitting lines and shape of the corresponding satellites comparable to electronic configuration of  $\text{Co}^{\text{II}}$  (Figure S17). Further analyses of the sample allowed also the identification of C ( $\text{sp}^2$ ), O and N as expected from the crystal structure and bulky analyses. Figure 9 shows the density of states (DOS) spectrum measured by means of UPS on spin-coated films of **2** on HOPG (red) compared to the calculated DOS spectrum (blue, Gaussian code<sup>36</sup> with the B3LYP functional<sup>37</sup> and the TZV basis<sup>38</sup>). The DOS of the clean substrate, a freshly cleaved HOPG surface (black), is also shown. The energy reference (0 eV) is set to the Fermi level of the experimental system, that has been previously determined with an in-situ cleaned Au(111) crystal.<sup>39</sup>

Note the remarkable agreement between experimental and calculated features at 2.1 and 3.8 eV that correspond to two sets of eight and seventeen molecular orbitals, respectively. These two first sets of orbitals contain mostly  $\pi$  anthracene orbitals. The  $e_g$  and  $t_{2g}$  orbitals are in the higher binding energy of the first and second band, respectively. Features at 7.6 and 8.6 eV are also reproduced by the calculations. The broad feature at about 6 eV is observed in both experimental and calculated spectra but it lies within the large feature arising from the HOPG substrate. Therefore, as a conclusion both experiments, XPS and UPS, show the expected patterns for compound **2**, confirming the stability of the sample under such conditions.

XPS experiments for compound **1** on the other hand, showed a clear absence of N on the HOPG surface and ambiguous results from the  $\text{Co}^{\text{II}}$  analysis. This is probably due to the loss of py molecules during of the deposition procedure, proving that compound **2** is a more robust system upon spin-coating, and clarifying the AFM experimental results for both systems. Importantly, this points out the necessity of photoemission studies on nanostructured systems toward their correct analysis.

### Conclusions

In summary, this work reports the two first crystallographically characterized mononuclear  $\text{Co}^{\text{II}}$ -CCMoid coordination compounds of the literature. Both systems, **1** ( $[\text{Co}(\text{9Accm})_2(\text{py})_2]$ ) and **2** ( $[\text{Co}(\text{9Accm})_2(2,2'\text{-bpy})]$ ), exhibit octahedral environments, containing two CCMoid ligands (9Accm) that bind one  $\text{Co}^{\text{II}}$  center together with two pyridine molecules or one 2,2'-bpy group, giving as a result *trans* (**1**) and *cis* (**2**) dispositions of the 9Accm ligands in the final arrangements. The use of microwave assisted organic reactions provided high yields and pure compounds. The "quasi-isomers" display comparable features and allow the study of the structural/magnetic/fluorescent similarities but also they show differences in solution and in the solid state. Paramagnetic  $^1\text{H}$  NMR studies of **1** and **2** show the stability of the systems in solution and allows the recognition of *cis/trans* Co-CCMoids by the downfield shift of the methine proton (-CH-) of coordinated 9Accm ligands. Furthermore, moderate emissions in the visible (related to the anthracene groups of

9Accm) have been found for both species in organic solvents despite the partial fluorescence quenching that both systems present given by the paramagnetic nature of the metal. **1** and **2** show solvatochromic effects with similar fluorescent yields. In the solid state, the two systems exhibit Single-Molecule Magnet behaviour, albeit only under applied *dc* fields, and constitute the newest additions to the limited family of mononuclear Co<sup>II</sup> hexacoordinated SMMs. Compound **1** presents one of the highest positive *D* values (*D* = +74 cm<sup>-1</sup>) found for mononuclear Co<sup>II</sup> systems and compound **2** shows only about a third of this value (*D* = +24 cm<sup>-1</sup>). This fact emphasizes the magnetic repercussion that has slight variations of the coordination sphere around the Co<sup>II</sup> center. These studies have been corroborated by CASSCF/NEVPT2 calculations, from which the positive *D* values for both systems have been obtained, being larger the anisotropy for **1** due to the existence of low-lying excited states closer in energy to the ground state. At last, deposition of **1** and **2** on HOPG and Si(100) substrates have been characterized. AFM images show the formation of aggregates of **1** and **2** on HOPG, showing the affinity of both species for such substrate, although XPS and UV photoemission studies demonstrate that only compound **2** is robust enough to form stable thin films on HOPG. For such system, the UV photoemission results are in excellent agreement with the theoretical calculations. Altogether, **1** and **2** present major differences in their magnetic performance in solution and in the solid state meanwhile fluorescent properties are comparable in solution. On the other hand, studies in solution depict the stability of both systems but deposition on graphene (by the use of spin-coating) points out the necessity of careful characterizations of molecules on surfaces, being **1** unstable under the experimental conditions and **2** the most robust system among the two described. In addition, we have introduced additional techniques as paramagnetic <sup>1</sup>H NMR, fluorescence and UV photoemission within the field of SMMs toward further analyses of functional molecular materials and therefore, their consideration in other areas related to nanoscience.

#### Acknowledgements

The authors thank Dr. N. Clos and Dr. G. Oncins from the UB for their great assistance. This work was supported by the MICINN (Spain) (Projects CTQ2012-32247, CTQ2011-23862-CO2-01, MAT2012-38319-CO2 and MAT2013-47869-C4-2-P). ICN2 acknowledges support of the Spanish MINECO through the Severo Ochoa Centers of Excellence Program under Grant SEV-2013-0295. ER thanks Generalitat de Catalunya (ICREA Academia). The Advanced Light Source (S. J. T.) is supported by the Director, Office of Science, Office of Basic Energy Sciences of the U. S. Department of Energy under Contract DE-AC0205CH11231.

#### Notes and references

- (a) E. Burzurí, R. Gaudenzi, H. S. J. Van der Zant, *J. Phys.: Condens. Matter* 2015, **27**, 113202(14pp). (b) B. J. Jung, N. J. Tremblay, M.-L. Yeh, H. E. Katz, *Chem. Mater.* 2011, **23**, 568-582. (c) R. M. Metzger, *J. Mat. Chem.* 2008, **18**, 4364-4396.
- (a) M. Verdaguer, V. Robert, *Comprehensive Inorganic Chemistry II: From Elements to Applications*, Elsevier: Amsterdam, 2013, **8**, 131-189. (b) J. M. Clemente-Juan, E. Coronado, A. Gaita-Ariño, *Chem. Soc. Rev.* 2012, **41**, 7464-

7478. (c) W. Wernsdorfer, *Int. J. Nanotech.* 2010, **7**, 497-522. (d) D. Gatteschi, R. Sessoli, J. Villain, *Molecular Nanomagnets*, Oxford University Press, Oxford, 2006.
- M. Castellano, R. Ruiz-García, J. Cano, J. Ferrando-Soria, E. Pardo, F. R. Foratea-Pérez, S.-E. Stiriba, M. Julve, F. Lloret, *Acc. Chem. Res.* 2015, **48**, 510-520.
- M. V. Kovalenko, L. Manna, A. Cabot, Z. Hens, D. V. Talapin, C. R. Kagan, V. I. Klimov, A. L. Rogach, P. Reiss, D. J. Milliron, P. Guyot-Sionnest, G. Konstantatos, W. J. Parak, T. Hyeon, B. A. Korgel, C. B. Murray, W. Heiss, *ACS Nano*, 2015, **9**, 1012-1057.
- (a) J. Narayan, *Int. J. Nanotech.* 2012, **9**, 914-941. (b) S. J. van der Molen, J. H. Liao, T. Kudernac, J. S. Agustsson, L. Bernad, M. Calame, B. J. van Wees, B. L. Feringa, C. Schonenberger, *Nano Lett.* 2009, **9**, 76-80.
- G. Kumar, R. Gupta, *Chem. Soc. Rev.*, 2013, **42**, 9403-9453.
- (a) U. Jayarathene, P. Chandrasekaran, A. F. Greene, J. T. Mague, S. DeBeer, K. M. Lancaster, S. Sproules, J. P. Donahue, *Inorg. Chem.* 2014, **53**, 8230-8241. (b) I.-R. Jeon, R. Clérac, *Dalton Trans.* 2012, **41**, 9569-9586. (c) L. J. Xu, G.-T. Xu, Z.-N. Chen, *Coord. Chem. Rev.* 2014, **273-274**, 47-62.
- C. Train, R. Gheorghe, V. Krstic, L.-M. Chamoreau, N. S. Ovanesyan, G. L. J. A. Rikken, M. Gruselle, M. Verdaguer, *Nat. Mater.* 2008, **7**, 729-734.
- N. Aliaga-Alcalde, L. Rodríguez, M. Ferbinteanu, P. Hofer, T. Weyhermüller, *Inorg. Chem.* 2012, **51**, 864-873.
- (a) K. S. Pedersen, J. Bendix, R. Clérac, *Chem. Commun.* 2014, **50**, 4396-4415. (b) T. E. O. Screen, J. R. G. Thorne, R. G. Denning, D. G. Bucknall, H. L. Anderson, *J. Mater. Chem.* 2003, **13**, 2796-2808.
- F. Pineider, M. Mannini, C. Danieli, L. Armelao, F. M. Piras, A. Magnani, A. Cornia, R. Sessoli, *J. Mater. Chem.* 2010, **20**, 187-194.
- (a) F. Prins, M. Monrabal-Capilla, E. A. Osorio, E. Coronado, H. S. J. van der Zant, *Adv. Mater.* 2011, **23**, 1545-1549. (b) M. L. Perrin, C. A. Martin, F. Prins, A. J. Shaikh, R. Eelkema, J. H. van Esch, J. M. van Ruitenbeek, H. S. J. van der Zant, D. Dulic, *Beilstein J. Nanotechnol.* 2011, **2**, 714-719.
- (a) B. S. Mendiguchia, I. Aiello, A. Crispini, *Dalton Trans.*, 2015, **44**, 9321-9334. (b) T. Esatbeyoglu, P. Huebbe, I. M. A. Ernst, D. Chin, A. E. Wagner, G. Rimbach, *Angew. Chem. Int. Ed.* 2012, **51**, 5308-5332.
- N. Aliaga-Alcalde, P. Marqués-Gallego, M. Kraaijkamp, C. Herranz-Lancho, H. den Dulk, H. Gerner, O. Roubeau, S. J. Teat, T. Weyhermüller, J. Reedijk, *Inorg. Chem.*, 2010, **49**, 9655-9663.
- F. Prins, A. Barreiro, J. W. Ruitenberg, J. S. Seldenthuis, N. Aliaga-Alcalde, L. M. K. Vandersypen, H. S. J. van der Zant, *Nano Letters*, 2011, **11**, 4607-4611.
- (a) M. Menelaou, T. Weyhermüller, M. Soler, N. Aliaga-Alcalde, *Polyhedron*, 2013, **52**, 398-405. (b) M. Menelaou, F. Ouharrou, L. Rodríguez, O. Roubeau, S. J. Teat, N. Aliaga-Alcalde, *Chem. – Eur. J.* 2012, **18**, 11545-11549. (c) N. Aliaga-Alcalde, L. Rodríguez, *Inorg. Chim. Acta*, 2012, **380**, 187-193.
- I. A. Gass, C. J. Milios, A. G. Whittaker, F. P. A. Fabin, S. Parsons, M. Murrie, S. P. Perlepes, E. K. Brechin, *Inorg. Chem.* 2006, **45**, 5281-5283.
- R. C. Elder, *Inorg. Chem.* 1968, **7**, 1117-1123.
- (a) T. B. Faust, P. G. Heath, C. A. Muryn, G. A. Timco, R. E. P. Winpenny, *Chem. Comm.*, 2010, **46**, 6258-6260. (b) E. C. Sañudo, T. B. Faust, C. A. Muryn, R. G. Pritchard, G. A. Timco, R. E. P. Winpenny, *Inorg. Chem.*, 2009, **48**, 9811-9818. (c) G. Aromí, A. S. Batsanov, P. Christian, M. Helliwell, O. Roubeau, G. A. Timco, R. E. P. Winpenny, *Dalton Trans.* 2003, 4466-4471. (d) E. C. Constable, C. E. Housecroft, T. Kulke, C. Lazzarini, *J. Chem. Soc., Dalton Trans.*, 2001, 2864-2871.

- 20 (a) W. J. Wang, H. H. Wei, *J. Chinese Chem. Soc.* 1978, **25**, 185-194. (b) J. A. Happe, R. L. Ward, *J. Chem. Phys.* 1963, **39**, 1211-1218.
- 21 K. Dimitrou, J.-S. Sun, K. Folting, G. Christou, *Inorg. Chem.* 1995, **34**, 4160-4166.
- 22 M. W. Wemple, H.-L. Tsai, K. Folting, D. N. Hendrickson, G. Christou, *Inorg. Chem.* 1993, **32**, 2025-2031.
- 23 M. L. Nicholas, R. S. Drago, *J. Am. Chem. Soc.* 1968, **90**, 2196-2197.
- 24 (a) M. Mameli, V. Lippolis, C. Caltagirone, J. L. Capelo, O. N. Faza, C. Lodeiro, *Inorg. Chem.* 2010, **49**, 8276-8286. (b) G. Zong, G. Lu, *J. Phys. Chem.* 2009, **113**, 2541-2546.
- 25 N. F. Chilton, R. P. Anderson, L. D. Turner, A. Soncini, K. S. Murray, *J. Comput. Chem.* 2013, **34**, 1164-1175.
- 26 (a) F. Habib, I. Korobkov, M. Murugesu, *Dalton Trans.* 2015, **44**, 6368-6373. (b) C. Plenck, J. Krause, E. Rentschler, *Eur. J. Inorg. Chem.* 2015, **2015**, 370-374. (c) S. Gómez-Coca, A. Urtizberea, E. Cremades, P. J. Alonso, A. Camon, E. Ruiz, F. Luis, *Nature Commun.* 2014, **5**, 4300. (d) M. S. Fataftah, J. M. Zadrozny, D. M. Rogers, D. E. Freedman, *Inorg. Chem.* 2014, **53**, 10716-10721. (e) R. Ruamps, L. Batchelor, R. Guillot, G. Zakhia, A.-L. Barra, W. Wernsdorfer, N. Guihery, T. Mallah, *Chem. Sci.*, 2014, **5**, 3418-3424. (d) R. Boča, J. Miklovič, J. Titiš, *Inorg. Chem.* 2014, **53**, 2367-2369. (f) Y.-Y. Zhu, C. Cui, Y.-Q. Zhang, H.-H. Jia, X. Guo, C. Gao, K. Qian, S.-D. Jiang, B.-W. Wang, Z.M- Wang, S. Gao. *Chem. Sci.*, 2013, **4**, 1802-1806. (g) F. Habib, O. R. Luca, V. Vieru, M. Shiddiq, I. Korobkov, S. Gorelsky, M. K. Takase, L. F. Chibotaru, S. Hill, R. H. Crabtree, M. Murgesu, *Angew. Chem. Int. Ed.* 2013, **52**, 11290-11293. (h) J. Vallejo, R. Ruiz-García, J. Cano, M. Julve, F. Lloret, G. De Munno, W. Wernsdorfer, E. Pardo, *J. Am. Chem. Soc.* 2012, **134**, 15704-15707. (i) T. Jurca, A. Farghal, P.-H. Lin, I. Korobkov, M. Murugesu, D. S. Richeson, *J. Am. Chem. Soc.* 2011, **133**, 15814-15817. (j) J. M. Zadrozny, J. R. Long, *J. Am. Chem. Soc.* 2011, **133**, 20732-20734.
- 27 S. Gómez-Coca, E. Cremades, N. Aliaga-Alcalde, E. Ruiz, *J. Am. Chem. Soc.* 2013, **135**, 7010-7018.
- 28 N. F. Chilton, R. P. Anderson, L. D. Turner, A. Soncini, K. S. Murray, *J. Comput. Chem.* 2013, **34**, 1164-1175.
- 29 F. Neese, E. I. Solomon, In *Magnetism: Molecules to Materials*; Miller, J. S., Drillon, M., Eds.; Wiley-VCH: Weinheim, 2003; Vol. 4, p 345.
- 30 (a) The so-called "magic pentagon" summarizes the result of the evaluation of the matrix elements and therefore the transitions that have repercussion for the Co<sup>II</sup>. (b) *Magnetism: Molecules to Materials (IV). Nanosized Magnetic Materials.* 2002 Wiley-VCH Verlag GmbH &Co. KGaA, page 387.
- 31 CC-FIT, Copyright©2014 Nicholas F. Chilton.
- 32 J. M. Zadrozny, M. Atanasov, A. M. Bryan, C.-Y. Lin, B. D. Rekker, P. P. Power, F. Neese, J. R. Long, *Chem. Sci.* 2013, **4**, 125-138.
- 33 X.-C. Huang, C. Zhou, D. Shao, X.-Y. Wang, *Inorg. Chem.* 2014, **53**, 12671-12673.
- 34 E. Cremades, E. Ruiz, *Inorg. Chem.* 2011, **50**, 4016-4020.
- 35 S. Jo, M. Takenaga, *J. Phys: Conf. Series* 2010, **258**, 012017.
- 36 J. Fraxedas, J. García-Gil, S. Monturet, S. Lorente, N. Fernández-Torrente, I. Franke, K. J. Pascual, J. I. Vollmer, A. Bluhm, R.-P. Koch N. and Ordejón, P. *J. Phys. Chem. C* 2011, **115**, 18640-18648.
- 37 J. Fraxedas, Y. J. Lee, I. Jimenez, R. Gago, R. M. Nieminen, P. Ordejón, E. Canadell, *Phys. Rev. B* 2003, **68**, 195115/1-11.
- 38 F. Mavandadi, A. Pilotti, *Drug Discov. Today*, 2006, **11**, 165-174.
- 39 M. Aghamohammadi, A. Fernández, M. Schmidt, A. Pérez-Rodríguez, A. R. Goñi, J. Fraxedas, G. Sauthier, M. Paradinas, C. Ocal, E. Barrera, *J. Phys. Chem. C*, 2014, **118**, 14833-14839.